CHAPTER 3

EXPERIMENTAL DETAILS

This chapter describes the properties of the materials used in the present study and the method to prepare gel polymer electrolyte. The detail theory is explained of experimental techniques used for characterization to investigate various properties viz., structural, thermal, and electrical properties, mechanical, and electrochemical properties of the polymer electrolytes.

3.1 Introduction

In the present chapter, the sample preparation method and experimental techniques have been described. Different experimental techniques have been applied to characterize different properties of prepared gel polymer electrolytes. X-ray diffraction (XRD), Fourier transform infrared spectroscopy (FTIR), Scanning electron microscope (SEM) and, Atomic force microscope (AFM) are used to study the structural and morphological properties of the prepared gel polymer electrolyte. Differential scanning calorimetry (DSC) investigates the thermal properties of the electrolyte. The electrochemical impedance spectroscopy technique is used to study the electrical properties of the electrolyte. Electrochemical studies are measured using cyclic voltammetry (CV) and linear sweep voltammetry (LSV). Wagner's DC polarization technique is applied to carry out a transport number of gel polymer electrolytes.

3.2 Sample Preparation

Various physical and chemical methods are available to prepare the polymer electrolytes which are listed here. (1) Solution cast technique (2) Hot press technique (3) Phase inversion method (4) Thermal evaporation technique (5) Laser evaporation technique (6) Sputtering.

Among all of the above preparation techniques, the solution cast technique is the traditional method due to the ease of preparation of polymer electrolyte fabrication of polymer in the form of film with high flexibility. It is also the cheapest and simplest method by which polymer can be shaped into the desired form. The procedure of solution cast technique is given in the form of a chart (Figure 3.1). In the first step, the polymer should be dissolved into a solvent and kept for stirring till the homogeneous mixture is obtained. In the obtained homogeneous solution, the required amount of salt is added and kept for stirring till the polymer-salt complexation is achieved. The main important thing is the solvent should be universal which is able to dissolve both, polymers as well as salt [1]. An organic solvent such as dimethylformamide (DMF), acetonitrile (ACN), acetone, tetrahydrofuran (THF) can be used. The addition of plasticizers or nano-filler can be incorporated in the required amount in the polymer-salt mixture and stirring should be done till the viscous solution is obtained. After that, the obtained viscous solution should be cast into Teflon or glass Petri dishes and left for the slow evaporation of solvent at or above room temperature for a few days. After that, a thin membrane of polymer electrolytes of uniform thickness can be achieved.

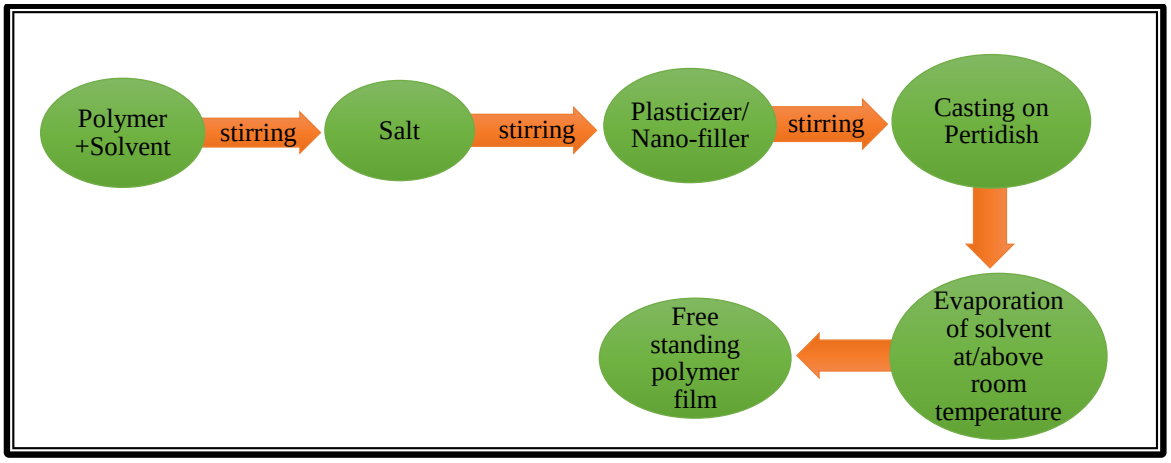

Figure 3.1 Solution cast technique in the form of a flow chart.

As far as the selection of host polymer is concerned, it should have an electron enrich group that helps for the more and more dissociation of ions and ion transport through the host polymer's coordinating sites. Also, the amorphous region should be present in the system and possible segmental motion of polymer chain in the polymer matrix should occur

[2]. In the present work, for gel polymer electrolyte, PVDF-HFP and PMMA as host polymers, $LiClO_4$ as ionic salt, organic solvent PC and DEC used as a plasticizer, and Al_2O_3 as nanofiller is used. Details of the used materials are given in Table 3.1 and briefly discussed below.

Table 3.1 Details of the materials used to prepare gel polymer electrolyte.

Sr. No.	Materials	Role	Structure	Molecular weight g/mol	Company
1	Poly (vinylidene fluoride - hexafluoro propylene) (PVDF-HFP)	Host polymer	$(-CH_2CF_2-)_x$ $[-CF_2CF(CF_3)-]_y$	400,000	Sigma Aldrich
2	Poly (methyl methacrylate) (PMMA)	Host polymer	$[CH_2C(CH_3)(CO_2CH_3)]_n$	350,000	Alfa Aesar
3	Propylene carbonate (PC)	Plasticizer	$C_4H_6O_3$	102.09	Sigma Aldrich
4	Diethyl Carbonate (DEC)	Plasticizer	$C_5H_{10}O_3$	118.13	Sigma Aldrich
5	Lithium perchlorate	Dopant salt	$LiClO_4$	106.39	Sigma Aldrich
6	Aluminium Oxide	Nano filler	Al_2O_3	101,96 (< 50nm)	Sigma Aldrich
7	Acetone	Solvent	C_3H_6O	58.08	Sulab lab

3.2.1 Materials

(1) Poly (vinylidene fluoride - hexafluoropropylene) (PVDF-HFP)

PVDF-HFP has received a lot of attention as a host polymer due to its excellent properties such as low degree of crystallinity and high dielectric constant $\varepsilon \approx 8.4$ that help in higher dissociation of lithium salt [3,4]. PVDF-HFP holds semi-crystalline nature. The PVDF-HFP polymer possesses both amorphous and crystalline phases in which the amorphous HFP part can trap a large amount of liquid electrolytes whereas the crystalline VDF part assists in the improvement of the mechanical stability for the formation of free-standing films [5].

(2) Poly (methyl methacrylate) (PMMA)

In the present work, along with PVDF-HFP polymer, PMMA is used as a blender polymer because of its beneficial properties viz., compatible nature with other polymers, high chemical and surface resistance, high ionic conductivity close to liquid electrolyte i.e. 10^{-3} S cm^{-1} at 25 °C, etc [6]. PMMA polymer is amorphous in nature. PMMA is not only a

lightweight and transparent polymer having lesser reactivity toward lithium metal-based anode but is predominantly insulating with only electronic transport behavior. It can be modified into an ionically conducting system because it comprises of two probable solvating hetero-atom/polar functional groups (i.e., C=O, O–CH) with electron-donating ability, which are important sites for cation coordination playing a crucial role in controlling conductivity level and determining the nature of the interaction of the ions with the polymer matrix.

(3) Plasticizers

The plasticizer is a low molecular weight organic solvent that has the ability to dissociate the salt and maintain the liquid state within the polymer matrix [7]. The dissociation of salt ions leads to increases in the number of free mobile ions which contribute toward the conductivity of polymer electrolyte. It also helps in increasing the amorphous phase in the polymer electrolyte. Moreover, the addition of plasticizers to GPE also softens the polymer backbone which results in high segmental motion that also assists the movement of ions. Hence, high dielectric permittivity and low viscosity are essential properties of plasticizers to promote ion-pair dissociation. A single plasticizer cannot fulfill the requirement of the above-mentioned properties, therefore, in the present study, the mixture of PC ($\varepsilon \approx 64.4$, viscosity at 25°C ≈ 2.53mPa S) and DEC ($\varepsilon \approx 2.82$, viscosity at 25°C ≈ 0.748mPa S) have been taken. Recently, many researchers have reported the various GPEs with various plasticizers to enhance the different properties such as ionic conductivity, structural properties, surface morphology, etc [8,9].

(4) Lithium perchlorate ($LiClO_4$)

Salt is the main component of the polymer electrolyte (PE) that provides conducting species to GPE. The ionic conductivity of polymer electrolyte depends on the number of charge species and transportation of salt ions that occur through the amorphous region. $LiClO_4$ salt is chosen because of its smaller ionic radius, smaller dissociation energy, and high solubility in most of the organic solvents [10]. The lithium perchlorate salt has been found as a potential candidate due to its attractive properties such as high ionic conductivity, anodic stability, and economical too [11].

Table 3.2 Chemical structures of used materials for the fabrication of gel polymer electrolytes (GPEs) along with their properties [12].

Materials	Structural formula	Melting point (°C)	Boiling point (°C)	Glass transition temperature (°C)	Dielectric constant (at 25 °C)
PVDF-HFP	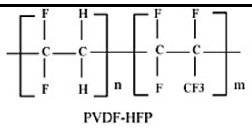 PVDF-HFP	142°C to 145°C	-	-65	8.4
PMMA	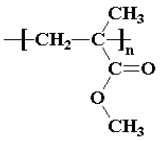	170	-	105	3.0
PC	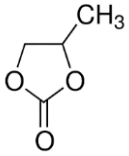	-54.53	242	-	64.95
DEC	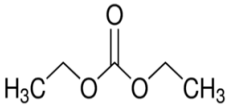	-43	126.8	-	2.82
$LiClO_4$	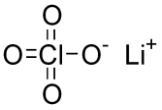	236	-	-24	-
Al_2O_3	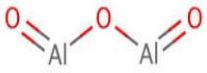	2045	2980	-	7.8
Acetone	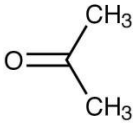	-94.7	56.29	-	20.56

(5) Aluminium Oxide (Al_2O_3) as nanofiller

It is believed that the electrical, mechanical, and electrochemical properties of the polymer electrolyte can be improved by adding nanofiller to the electrolyte system [13]. Specially, in the electrolyte system, the presence of a large amount of plasticizers causes loss of mechanical strength. Also, improvement in ionic conductivity is accompanied by a degradation in mechanical strength, poor compatibility and high reactivity with lithium electrode affect seriously the overall functionality of the device. All such properties can be improved by incorporating a small amount of nanoparticles in the gel polymer electrolytes system based on the interaction of Lewis acid-base theory [14]. As a nanofiller, Al_2O_3 is used due to its hydrophilic nature, high dielectric constant [15], and large surface area. It is

an electrically insulating and passive filler. Hence, it does not take part in the conduction process.

(6) Acetone as a solvent

Generally, the solvent is an organic solvent (carbon-containing) which plays a vital role in the fabrication of polymer electrolyte. It is a colorless liquid and a solvent should possess the properties such as low melting temperature, high boiling point, low viscosity, easy evaporation, non-toxic, economical, safe. It should have a high dielectric constant as well for easy dissolution of salt and polymer.

The chemical structures of the materials used to prepare GPE films along with their properties are listed in Table 3.2.

Various Polymer Electrolyte Systems

The gel polymer electrolyte systems were prepared with different concentrations of $LiCLO_4$ salt (Series (a)), PC: DEC (Series (b)), and Al_2O_3 nano-filler (Series (c)). To prepare the various polymer electrolyte system, the individual constituents were taken in weight percentage (wt.%) which is specified in Table 3.3, Table 3.4, Table 3.5.

Table 3.3 The composition of GPE system with different concentrations of $LiClO_4$ salt–Series (a).

Sr. No.	Sample code	PVDF-HFP (wt.%)	PMMA (wt.%)	PC+DEC (wt.%)	$LiClO_4$ (wt.%)
1	S1	24.5	24.5	49	2
2	S2	24	24	48	4
3	S3	23.75	23.75	47.5	5
4	S4	23.12	23.12	46.25	7.5
5	S5	22.5	22.5	45	10

Table 3.4 The composition of GPE system with different concentrations of PC: DEC plasticizers – Series (b)**.**

Sr. No.	Sample code	PVDF-HFP (wt.%)	PMMA (wt.%)	$LiClO_4$ (wt.%)	PC+DEC (wt.%)
1	P1	36.0	36.0	8	20
2	P2	31.5	31.5	7	30
3	P3	27.0	27.0	6	40
4	P4	22.5	22.5	5	50
5	P5	18.0	18.0	4	60

Table 3.5 The composition of nanocomposite GPE system with different concentrations of Al_2O_3 nanofiller – Series (c).

Sr. No.	Sample code	PVDF-HFP (wt.%)	PMMA (wt.%)	$LiClO_4$ (wt.%)	PC+DEC (wt.%)	Al_2O_3 (wt.%)
1	N1	17.91	17.91	9.95	53.73	0.5
2	N2	17.82	17.82	9.9	53.46	1
3	N3	17.64	17.64	9.8	52.92	2
4	N4	17.46	17.46	9.7	52.38	3
5	N5	17.28	17.28	9.6	51.84	4

3.2.2 Preparation of Gel Polymer Electrolyte

The Solution cast method has been adopted for the preparation of gel polymer electrolyte in the present work [16].

Solution Casting Method

An appropriate amount of PVDF-HFP and PMMA were completely dissolved separately in acetone using a magnetic stirrer for 2 hours until the solution gets clear transparent.

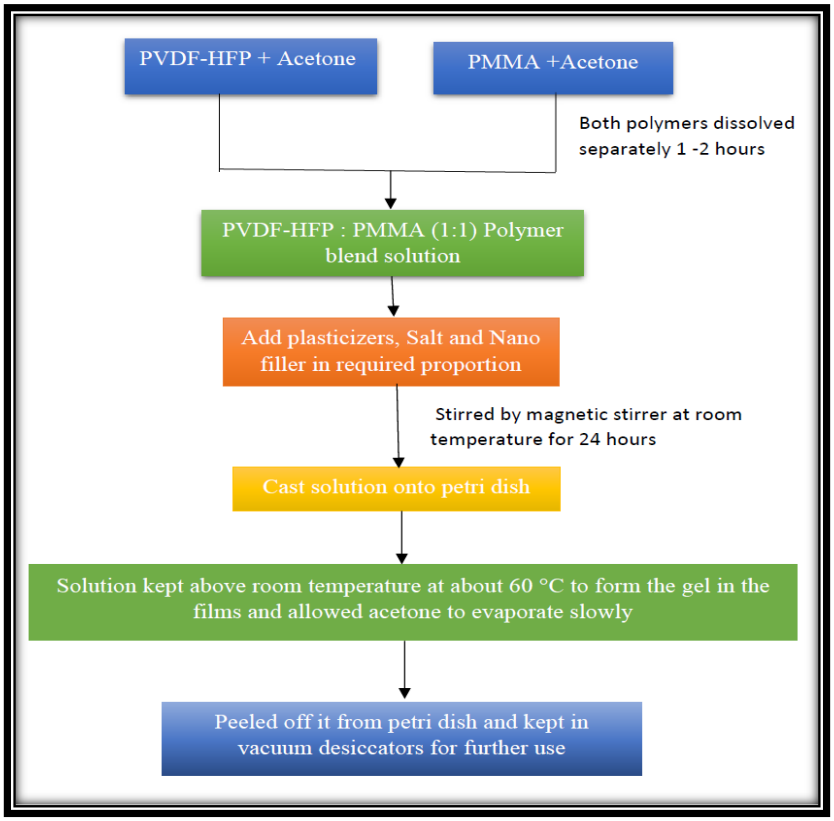

Figure 3.2 Flow chart for preparation of gel polymer electrolyte

The amount of PVDF-HFP and PMMA are taken in an equal ratio (1:1). Then Addition of $LiClO_4$ salt, PC: DEC plasticizers, and Al_2O_3 nanofiller is added in the required proportion

to prepare all series. And the solution was stirred for 24 hours until the mixture gets homogeneous in nature. After that, the solution is cast onto a Teflon Petri dish. All samples were kept above room temperature at about 60 °C to form the gel in the films and allowed acetone to evaporate slowly. After the evaporation of acetone, free-standing and flexible thin films of the thickness of about 0.12–0.14 mm were peeled off and kept in vacuum desiccators. The films were used for different experimental studies. The solution casting method to prepare gel polymer electrolyte is also shown in the form of a flow chart as shown in Figure 3.2. Figure 3.3 shows the prepared film and its flexibility.

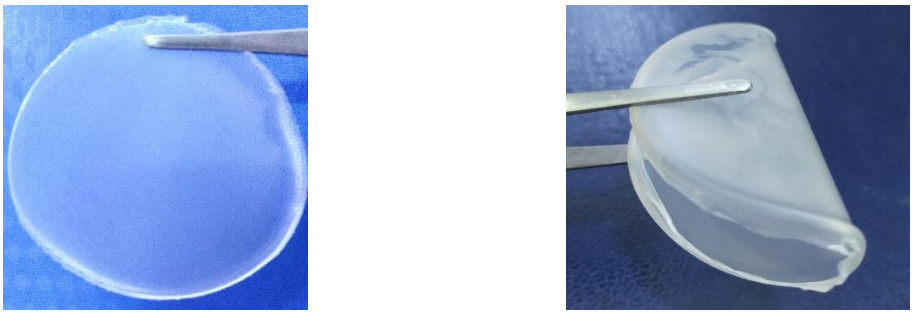

Figure 3.3 Photographs of gel polymer electrolyte (GPE) film.

3.3 Characterization Techniques

The theoretical details of various characterization techniques used to characterize prepared films are discussed below.

3.3.1 X-ray Diffraction (XRD)

X-ray diffraction is a non-destructive technique for characterization of the crystalline and amorphous materials [17]. It provides information on structures of the materials and other structural parameters such as average spacings between layers, the orientation of a single crystal, crystal defect, average grain size, crystallinity [18]. X-ray diffraction is based on the constructive interference of monochromatic x-rays from a crystalline sample. The x-ray peaks are produced by interference (constructive) of X-rays (monochromatic beam) scattered at a particular angle from each lattice plane of a sample and intensity of peak are recorded according to atomic position within the lattice planes of the material. This XRD pattern is the fingerprint of periodic or non-periodic atomic arrangement within the material.

When the accelerated electron strikes a metal target, such as copper, the energy is released as X-radiation due to the transition of the electron. The source and detector move on the circumference of the focusing circle with the sample stage at the center of the circle as shown in Figure 3.4.

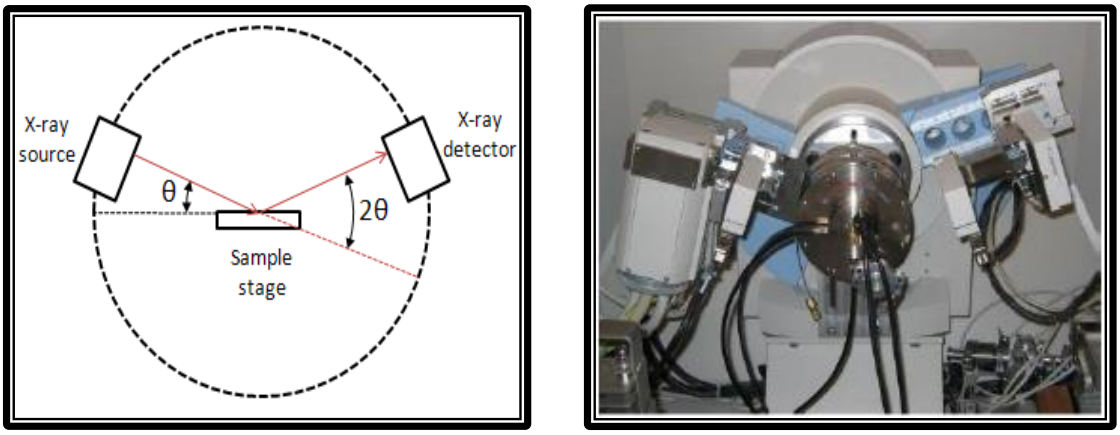

Figure 3.4 Schematic diagram and real view of XRD

Bragg's law [19] is used to make an accurate measurement of experimental results to determine the crystal structures. The angle between the plane of the specimen and the X-ray source θ is known as Bragg's angle and the angle between the projection of X-ray and the detector is 2θ. The X-ray diffractometer also consists of a goniometer which is used to maintain the angle and rotate the sample. The sample is mounted on the holder. The X-ray incident on the sample is scattered by each atom in a plane (lattice plane) of the sample. The detector records the number of XRD peaks at each angle of 2θ. The intensity of the X-ray beam is usually recorded as count per second. As shown in Figure 3.5, the reflection of X-ray from the lattice planes with interplanar distance 'd' of the sample produces constructive interference when satisfies Bragg's equation [20,21],

$$n\lambda = 2dsin\theta \tag{3.1}$$

where λ is the wavelength of X-ray, θ is the angle of diffraction and n is the order of diffraction. Using this Eq. 3.1, interplanar distance (d) can be measured. In the crystalline material, the atoms are arranged in a periodic array with long-range order so they can produce a diffraction pattern with sharp and intense peaks. Whereas in amorphous materials, the atom does not have long-range order with the periodic arrangement so they cannot produce diffraction pattern rather it produces X-ray scattering pattern with poorly defined peak called "humps" and broad in nature. This method is an important technique for the characterization of electrolyte films. It gives a very broad range of information about the

materials such as crystalline or amorphous nature. In the present work, x-ray diffraction studies have been carried out on the polymer, salts, and their complexes.

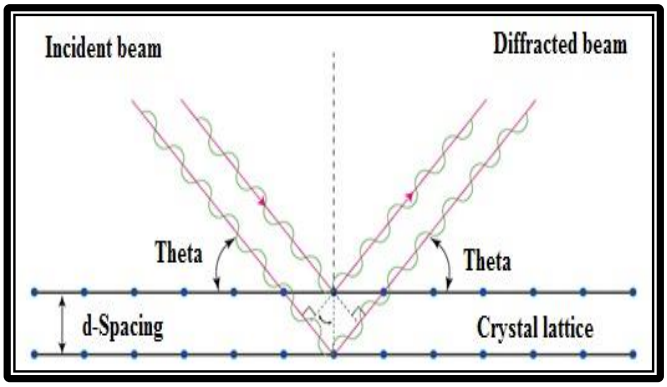

Figure 3.5 Diffraction in crystalline materials having lattice parameter (d)

In the present study, the XRD spectra of pure PVDF-HFP, pure PMMA, Pure $LiClO_4$ pattern, and prepared gel polymer electrolyte system were carried out to investigate the structural information of the materials. XRD pattern is recorded by BRUKER D2-Phaser (Figure 3.6) with Cu-Kα radiation of wavelength = 1.540 Å in 2θ range of 5 – 70° with a step of 0.05°.

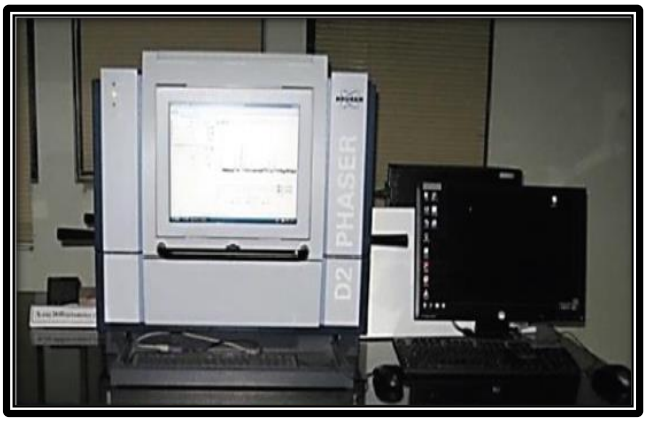

Figure 3.6 BRUKER D2-Phaser

3.3.2 Fourier Transform Infrared Spectroscopy (FTIR)

Infrared spectroscopy is a non-destructive as well as a rapid technique for the characterization of the polymer as it provides vital information about the presence of functional group as well any change due to salt or plasticizer in the polymer. FTIR spectroscopy is used to identify types of chemical bonds in a molecule by producing the absorption of the incident electromagnetic spectrum in the infrared region, which serves as

a molecular "fingerprint". IR is measured on free-standing polymer films or pallets which are made from a very small amount of (1or 2 mg) KBr powder material. The principle of this technique is that molecular bonds vibrate at various frequencies depending on the atoms or ions, types of bonds, and modes of vibration. When the frequency of IR radiation is equal to the vibrational frequency of molecules incident on the substance, it absorbs incident radiation and excites the molecules to a higher energy state. The energy of a vibration mode is given by

$$E_V = (V + \frac{1}{2})2h\upsilon \tag{3.2}$$

where Ev = energy of the V vibrational level, V = 0,1,2,3….

h = plank's constant (6.626×10^{-34} Js)

υ = frequency of vibration

It is used for the identification of organic molecules along with the interactions of different functional groups with the help of absorption/transmission spectra available in the complex polymeric spectra [22]. The infrared range of the electromagnetic spectrum is divided into three different regions [23].

1. Near-infrared (14000 – 4000 cm^{-1})
2. Mid-infrared (4000 – 400 cm^{-1})
3. Far-infrared (400 – 10 cm^{-1})

The mid-infrared region of the electromagnetic spectrum is used to study the fundamental vibrations and associated rotational and vibrational structures. By absorbing incident infrared radiation by a molecule, the electric dipole moment changes and causes the molecule to vibrate at a higher amplitude. Several different modes of stretching and bending vibrations (given below) may be responded to by a molecule after absorbing infrared radiation of a particular frequency [24]. The different modes of vibration are shown in Figure 3.7.

Stretching vibration	**Bending vibration**
(a) Symmetric stretching vibration	(a) Scissoring
	(b) Rocking
(b) Asymmetric stretching vibration	(c) Wagging
	(d) Twisting

The optical block diagram of FTIR is shown in Figure 3.8. The infrared radiation produced by a coherent source travels towards a half-silvered mirror also called a beam splitter and splits into two paths. Out of the split-beam, one moves towards the movable mirror and another beam towards the fixed mirror. Then these two rays recombine back onto the beam splitter this recombined beam passes through the sample. The path of one beam is of fixed length due to fix mirror whereas the other constantly changes by the movable mirror. The resulting signal interfere with each other and summation of constructive and destructive

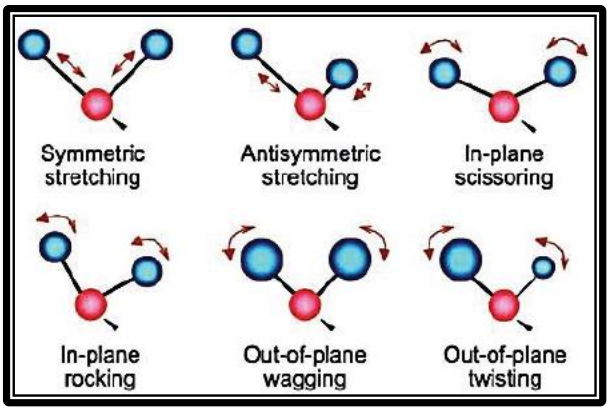

Figure 3.7 Modes of vibration

interference called an interferogram. A spectrum is obtained by measuring all frequencies via a technique called Fourier transform. When the radiation passes through the sample, some of the radiation is absorbed and some transmitted through which yield the transmittance spectrum. The spectrum where transmittance (%T) against wavelength (cm^{-1}) is recorded [25]. The transmittance is given by

$$T = \frac{I}{I_0} \tag{3.3}$$

where I represents transmitted light and I_0 is the incident light.

In the polymer chain, the repeat unit of the same group of atoms is present, hence it gives the same absorption/transmission peak. At higher frequencies above 1000 cm^{-1}, the peaks are obtained for the bonds between light atoms, like C–H, N–H, O–H and double bonds or triple bonds such as C=C, C=N, C=O, and C≡N. In the lower frequencies range below 1000 cm^{-1} called the fingerprint region, the peaks are characteristics of the molecules as a whole. It contains many bonds due to bending, vibration, skeletal vibrations, and C–C, C–O, C–N stretching vibrations. The interpretation of organic molecules with interaction with different functional groups is represented in the graphical form given in Figure 3.9.

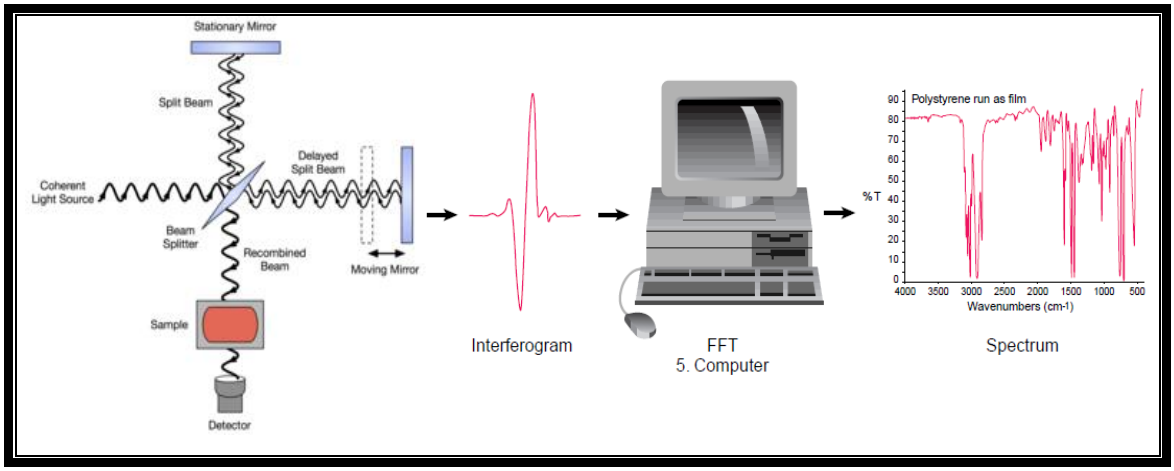

Figure 3.8 Optical diagram of Fourier transform infrared spectroscopy.

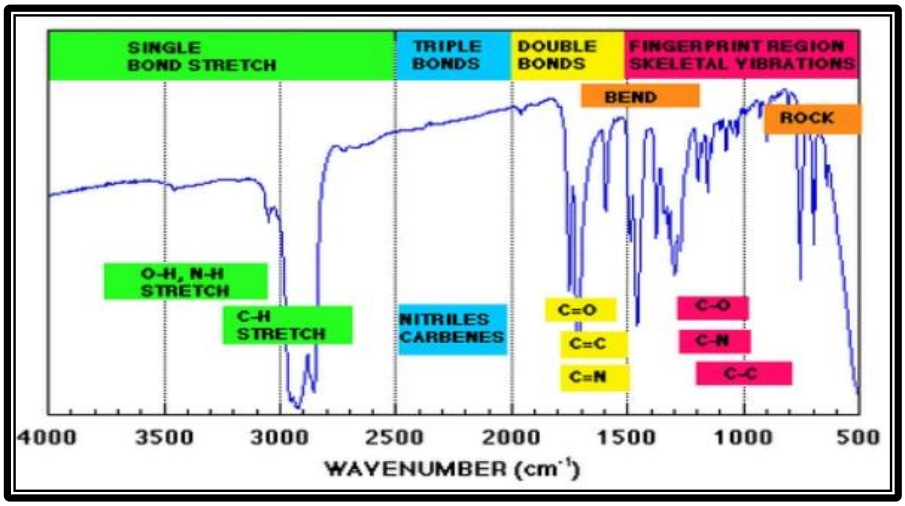

Figure 3.9 Interpretation of Infrared spectra.

Figure 3.10 FTIR 4100 JASCO model.

In the present study, FTIR characterization has been carried out to investigate ion-polymer interaction and possible changes in the functional group due to the addition of $LiClO_4$ salt,

PC:DEC plasticizers, and nano-filler dispersion in the host polymer. The FTIR spectra were recorded by using FTIR 4100 JASCO model (Figure 3.10) in the wavenumber range 400-4000 cm^{-1} with a resolution of 8 cm^{-1}.

3.3.3 Differential Scanning Calorimetry (DSC)

On heating, polymers undergo changes such as glass, crystallization, melting of polymer, and chemical changes such as decomposition, oxidation, etc. Hence, it is worth recording these changes and specific heat with respect to temperature. The thermal behavior of electrolyte systems can be analyzed using different thermal analysis techniques such as thermogravimetry analysis (TGA), differential thermal analysis (DTA), differential scanning calorimetry (DSC) [26]. DSC technique was introduced by Watson et al. to carry thermal analysis out of these all techniques [27]. DSC provides information on glass transition temperature (T_g), crystallization temperature (T_c), and melting temperature (T_m).

DSC technique measures heat flow or heat capacity as a function of temperature [28-30]. The schematic diagram of the DSC technique is shown in Figure 3.11. The experimental arrangement consists of two pans one for the sample and the other is reference pan [31]. Both pans are made up of aluminum out of which, sample pan contains about 1-2 mg sample is sealed by using crimper machine whereas reference pan contains Al_2O_3. The pans are heated separately in a sealed chamber where the temperature difference is kept at zero means during the thermal event, the sample transfers heat to and fro from the sample pan to maintain the same temperature. To achieve this, the sample and reference pan need extra heat. During the heat flow process, the sample may either absorb or release heat called an endothermic or exothermic reaction occurring in the sample [28]. Heat flow associated with the material transition as a function of temperature is recorded. This results in a definite pattern called a DSC thermograph.

It provides quantitative as well as qualitative data on the endothermic (heat absorption) and exothermic (heat evolution) processes of materials during the physical transition. This is caused by phase-changing or thermal transition such as melting of crystalline polymer, glass transition, and crystallization process. In the case of a polymer, both crystalline and amorphous phases are exhibited. Depending on the temperature, polymer shows different states such as brittle, glassy, elastic, or viscous liquid. The temperature below which polymer shows glassy means hard and brittle in nature and above it, the polymer is in a rubbery state, called **"Glass transition temperature (T_g)**", where it exhibits segmental

motion and flows freely. In another way, the glass transition temperature is defined as a change in the heat capacity as the polymer matrix goes from the glassy state to a rubbery state. Mechanical behavior of polymers changes at the glass transition temperature. The temperature at which polymer takes to transition from semi-crystalline phase to amorphous phase called **"Melting temperature (T_m)"**. A typical DSC plot of a polymer is shown in Figure 3.12.

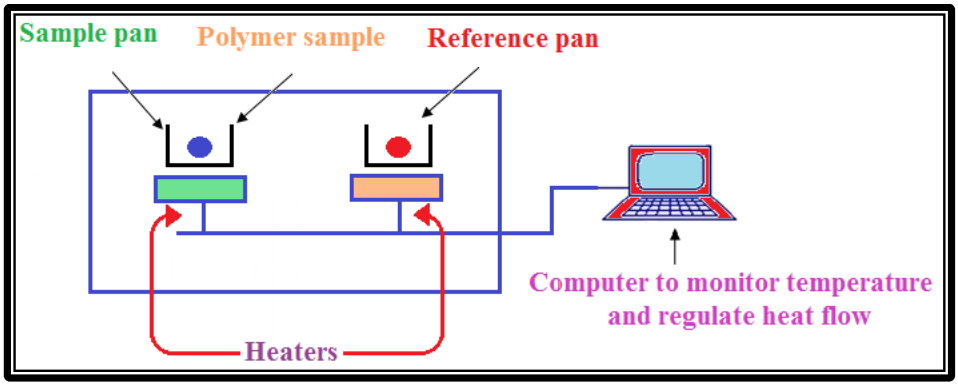

Figure 3.11 Schematic diagram of the DSC technique [32].

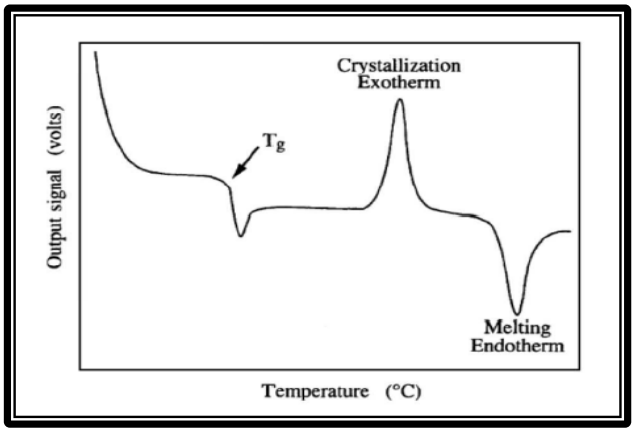

Figure 3.12 Typical thermograph of thermal analysis [32].

Only T_m and T_g are shown for polymers while glass system exhibits T_g, T_c and T_m. However, polymers with both crystalline and amorphous domains will show all the features, as shown in Figure 3.12. The thermal transition is recorded as positive and negative peaks which represent exothermic and endothermic reactions respectively.

In the current study, for the DSC measurement, the sample amount was taken around 1.5 mg - 2 mg and sealed in the aluminum pan using a crimpier machine. Thermal analysis of pure PVDF-HFP, pure PMMA, PVDF-HFP:PMMA blend, and different gel polymer

electrolytes have been carried out using the SII EXSTRAR 6000 model (Figure 3.13) with a heating rate of 10 °C/min.

Figure 3.13 SII EXSTAR 6000 DSC model.

3.3.4 Scanning Electron Microscope (SEM)

A scanning electron microscope produces images of a sample by scanning the surface with a focused beam of electrons [33]. The signals obtained from electron-sample interactions reveal information about the sample including external morphology, chemical composition, and crystalline structure [34]. The scanning electron microscope technique is used to carry out the morphology structural properties of materials [35].

Working principle

In the scanning electron microscope, the specimen is subjected to a focused electron beam from an electron gun, which scans the surface of the specimen. This gives rise to the release of secondary electrons and is detected by a detector and converted into electronic signals and produce an image on the cathode ray tube (CRT) [36].

A typical schematic diagram of SEM is shown in Figure 3.14. As seen from Figure 3.14, at the top of the microscope column, the primary monochromatic electron beam is produced from the electron gun with filament cathode. The released electron beams are accelerated between anode and cathode by a voltage of 0.5 kV to 30 kV. The vacuumed chamber is required to concentrate electron towards the sample to prevent from being scattered or disperse due to their interaction with the surrounding atmosphere or with other gas molecules. A beam of accelerated electrons travels through a vacuumed chamber and

passes through condenser lenses to adjust the electron beam spot size to produce a sharp image. Therefore, beams are allowed to pass through the first condenser lens consists of a condenser aperture which condenses the stream of the electron beam, eliminates some high-angle electron beam as well as limits the current along with it. After this, the beam passes through the second condenser lens which produces a coherent beam, and the electron beam is being focused towards scanning coils. The scanning coils where the electron beams are scanned for a certain time as per scanning speed. Thereafter, the electron beams are subjected towards the objective lens where it gets de-magnifies in terms of cross-section and then focuses with the diameter of nanometre-scale (of about 50 Å to 100 Å) on the surface of the sample.

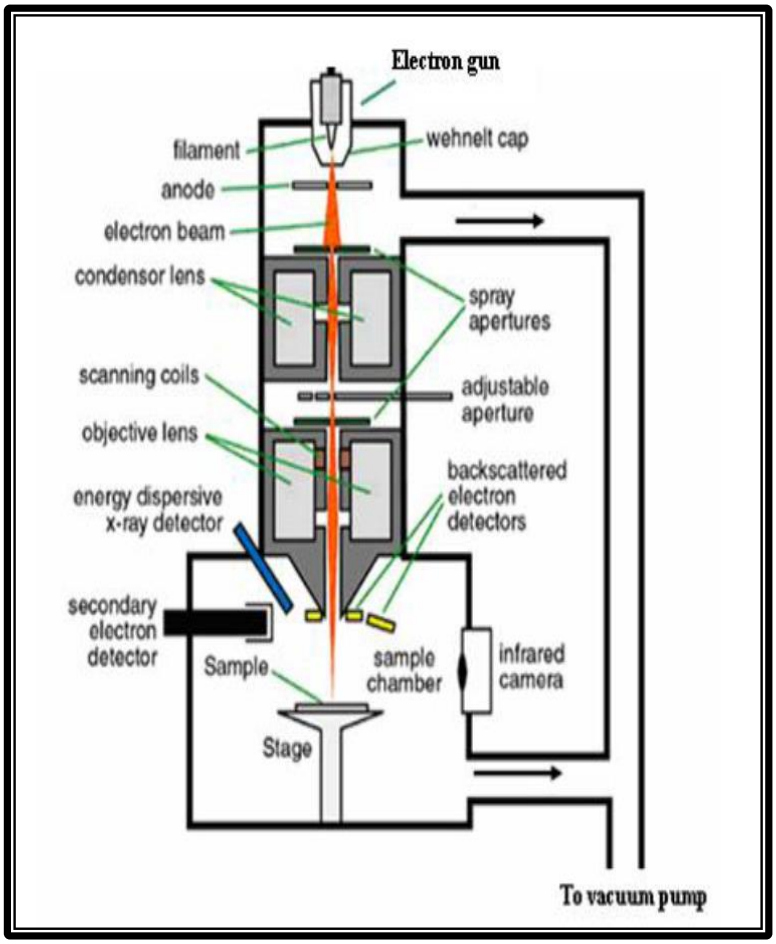

Figure 3.14 Schematic diagram of SEM.

In the present work, the structural morphology and surface properties of the prepared films are examined by a JEOL JSM-6010LA SEM (Figure 3.15).

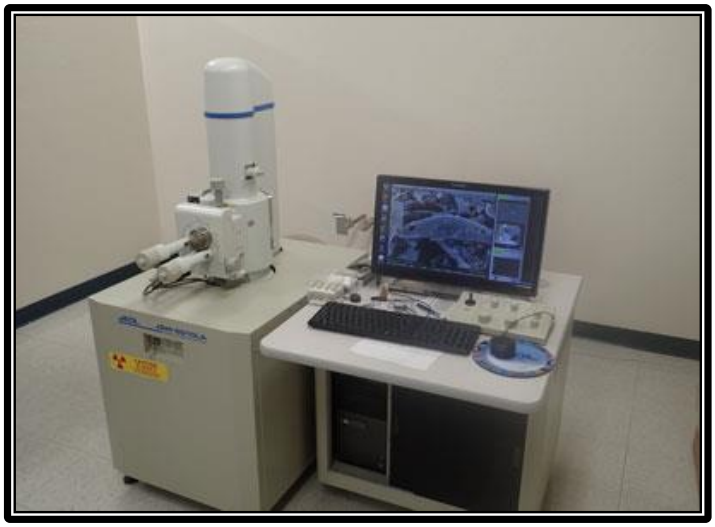

Figure 3.15 JEOL JSM-6010LA SEM Model.

3.3.5 Atomic Force Microscopy (AFM)

Atomic force microscope is also known as a scanning probe microscope. It measures various properties of the material by bringing the tip of the cantilever to be scanned over the surface of the specimen. Atomic force microscope gives the resolution of the order of a fraction of nanometre. The cantilever generally measures the deflection of the cantilever by using the optical lever. It can be operated in two modes. (1) Contact mode (2) Tapping mode. In contact mode, the tip is dragged over the surface of the specimen, and deflection of the cantilever and tip is measured by the laser beam and the information is compiled into a topography image. In the tapping mode, the tip of the cantilever is not touched to the surface of the specimen and kept in such a way that the force between the tip of the cantilever and the surface of the specimen remains constant by adjusting the height of the cantilever using a feedback loop. The schematic block diagram of the working of the Atomic force microscope is shown in Figure 3.16.

In the present work, AFM has been carried out to investigate the surface topology by using “Easy scan 2 AFM version 2.0 Nanosurf ” (Figure 3.17).

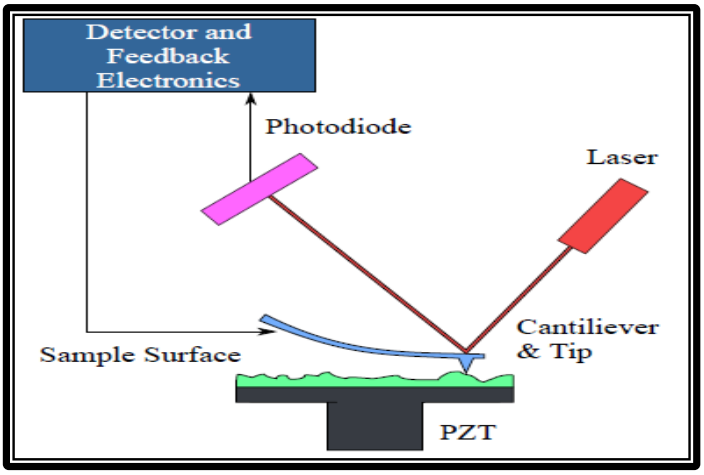

Figure 3.16 Block diagram of working of Atomic force microscope (AFM).

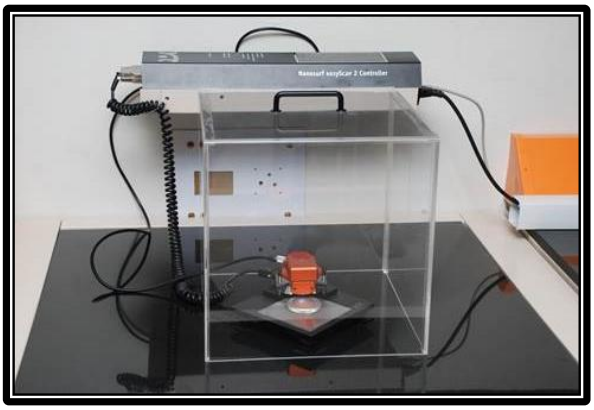

Figure 3.17 Easy Scan 2 AFM version 2.0 Nanosurf

3.3.6 Ionic Transport Number

For the use of polymer electrolytes in electrochemical devices, it is important to know the total ionic transference number of polymer electrolytes [38]. Electrical conductivity analysis gives the total ionic conductivity and ion transport mechanism in GPE, but it does not provide any information on the amount of current carried by ions. In a polymer electrolyte system, both anion and cation and free electrons are expected to move under the application of DC voltage and contribute to the conduction process [39]. For electrochemical applications, the ionic current contribution in the total conductivity of gel polymer electrolyte is crucial because the ions are moving charge carriers that play a vital role in device performance [40]. The experimental technique called "Transport number measurement" really helpful to understand whether the conduction process is due to the movement of ions or electrons. As polymers electrolytes are electronic insulators, the major

contribution in the conduction process should be of the ions. So, to know this ionic transport number is of great interest. The expression for the ionic transport number is

$$t_i = \frac{\sigma_i}{\sigma_t} = \frac{i_i}{i_t} \tag{3.4}$$

where t_i is ionic transport number, σ_i and σ_t are conductivity due to ions and total conductivity (ionic + electronic), respectively. i_i and i_t are current due to ions and total current (ionic + electronic). For a pure ionic conductor, $t_i = 1$ and $t_e = 0$ should be obtained. However, for the mixed ionic conductor (ionic as well as electronic conduction), the ionic transport number will be less than 1. In such cases, the ionic number t_i is given as

$$t_i = \frac{i_t - i_e}{i_t} = 1 - \frac{i_e}{i_t} = 1 - t_e \tag{3.5}$$

where t_e is electronic transport number and i_e is current due to electrons.

The ionic transport number can be measured by using different methods which include Wagner's polarization techniques [41], EMF measurement [42], Potentiostatic polarization, Tubandt's method [43], and DC polarization technique [44], Combined ac/dc technique [45].

3.3.6.1 Wagner Polarization Technique

This technique was first used by Wagner [46] to identify the contribution of ion and electron on the conductivity of the materials. In this technique, the reversible as well as blocking electrode used to sandwich the sample and DC potential applied across it. This method is known as Wagner's polarization technique after the method proposed by Wagner. When DC potential is applied across it, the mobile ionic species move towards the respective electrode. The experimental arrangement for the measurement of the ionic transference number is shown in Figure 3.18. Due to the blocking electrodes, the current becomes steady after some time. The typical curve for the current versus time is shown in Figure 3.19.

As the polarization build-up, the ions are blocked and the final current is steady that is due to electrons only. The initial current decreases with an increase in time due to the depletion of ionic species and becomes constant in a fully depleted situation. The initial current is the total current (i_t) which is due to the ions as well as the electron, whereas the final current

(steady current) with increasing time is due to electron only known as electronic current. The ionic transference number can be calculated from the total current and electronic current [47]. Eq. 3.4 gives the total ionic transference number (cationic + anionic + electronic).

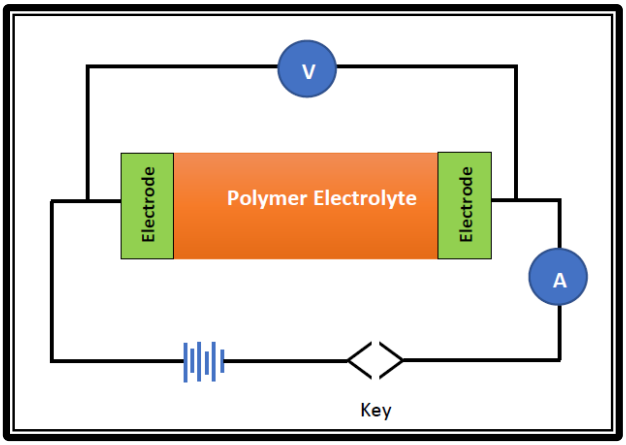

Figure 3.18 Experimental arrangement for Wagner's polarization method.

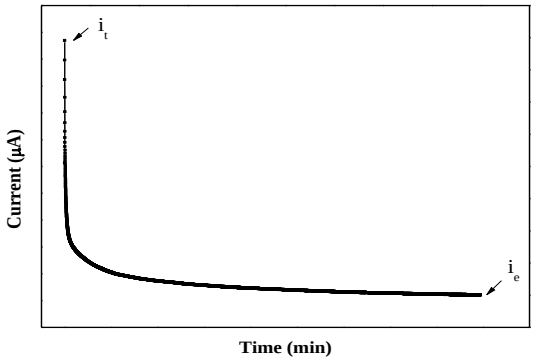

Figure 3.19 Typical DC polarization current versus time.

3.3.6.2 Combined ac/dc Technique for Cation Transport Number (t_+) / DC Polarization Technique.

A combined ac/dc technique for the measurement of cationic transport number was proposed by Vincent and co-workers [45]. A small voltage ΔV = 20 mV was applied to polarize the electrochemical cell Hg|polymer electrolyte film|Na-Hg. The initial current I_0 and final current Is were recorded.

The impedance measurement was done before and after the polarization for the evaluation of resistance which was recorded as R_0 and Rs respectively. And the cationic transport number (t_+) was calculated using the following formula.

$$t_+ = \frac{I_s(\Delta V - I_0 R_0)}{I_0(\Delta V - I_s R_s)} \tag{3.6}$$

3.3.6.3 EMF method

In this method, the ion-conducting material is placed between a pair of electrodes having different electrochemical potentials μ_1 and μ_2. The potential difference (emf) is developed across the cell is given by [48]

$$E_{measured} = \frac{-1}{|Z|F}\int_{\mu_1}^{\mu_2} t_i d\mu = \frac{t_i(\mu_1 - \mu_2)}{|Z|F} = \frac{t_i \Delta G}{|Z|F} \tag{3.7}$$

where t_i – ionic transference number,

μ_1 and μ_2 – chemical potential of electrodes,

ΔG – change in free energy for a pair of electrodes,

$|Z|$ – valance of mobile ion and,

F – Faraday's constant.

The theoretical emf is given by

$$E_{theoretical} = \frac{\Delta G}{|Z|F} \tag{3.8}$$

Hence,
$$E_{measured} = t_i E_{theoretical} \tag{3.9}$$

The transference number t_i can be calculated using this relation by taking the ratio of measured and theoretical emf values.

Among all these methods, Wagner's polarization technique is adopted for the measurement of the transference number. For the measurement, Keithley model 6514 electrometer interfaced with the computer is used to measure current as a function of time. The prepared gel polymer electrolytes were sandwiched between stainless steel blocking electrodes and dc bias of constant voltage was applied to the sample. The current flowing through the sample was measured as a function of time using Keithley model 6514 electrometer interfaced with the computer.

3.3.7 Cyclic Voltammetry (CV) and Linear Sweep Voltammetry (LSV)

It is important to measure the electrochemical stability window to know the utility of the polymer electrolyte as a separator in a battery. It can be evaluated by using cyclic voltammetry and linear sweep voltammetry. Cyclic voltammetry (CV) is a widely used and versatile electrochemical technique that provides qualitative information regarding electrochemical reactions such as the redox process and electron-transfer reaction [49]. The experimental setup of cyclic voltammetry consists of a potentiostat and three electrodes i.e. a working electrode, a counter electrode, and a reference electrode. The current at the working electrode is measured as a function of applied voltage which swept linearly with time between working and reference electrodes, while the reference electrode maintains a constant potential. The counter electrode conducts electricity from the signal source to the working electrode. The working electrode is the electrode where the oxidation and reduction process occurs which is recorded as a peak in the current signal. The peak at which the species begins is oxidized and reduced. The purpose of the electrolyte is to provide ions to the electrodes during oxidation and reduction.

In potential step measurement, the potential varies linearly of a stationary working electrode, using a triangular potential waveform as shown in Figure 3.20. In the case of LSV, the potential is scanned from a lower voltage value (V_1) to an upper limit (V_2), where, in CV, the potential is swept between two voltages (V_1 and V_2) at a fixed rate. When the voltage reaches V_2, the scan gets reversed and the voltage is swept back to V_1 at a fixed rate with a particular number of cycles. The current is measured as a function of voltage. The resulting current-voltage (I-V) plot is referred to as cyclic voltammogram depicted in Figure 3.21. From the plot, the various parameter can be measured such as the magnitude of anodic current (i_{pa}) and cathodic current (i_{pc}) and corresponding anodic peak potential (E_{pa}) and cathodic peak potential (E_{pc}) respectively. A species may be oxidized i.e. transfer of an electron from the electrolyte to the electrode when the potential of the working electrode is more positive than that of the oxidation potential of the redox couple. This transfer of electrons produces a current called anodic current represented by (i_{pa}). When the potential scan is reversed, a species may be reduced i.e. electrons transfer is away from the electrode, and the potential of the working electrode is more negative than that of the reduction potential of the redox process. This produces a current called cathodic current which is represented by i_{pc}.

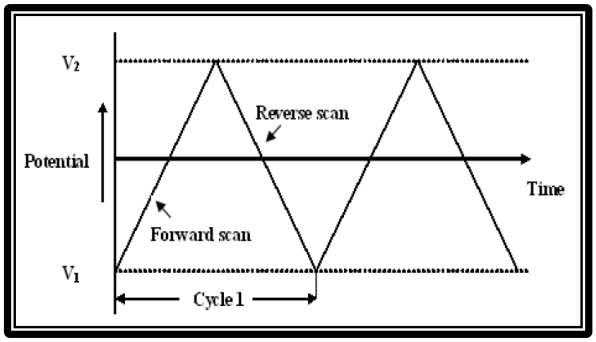

Figure 3.20 Signal applied in cyclic voltammetry: Potential as a function of time [50].

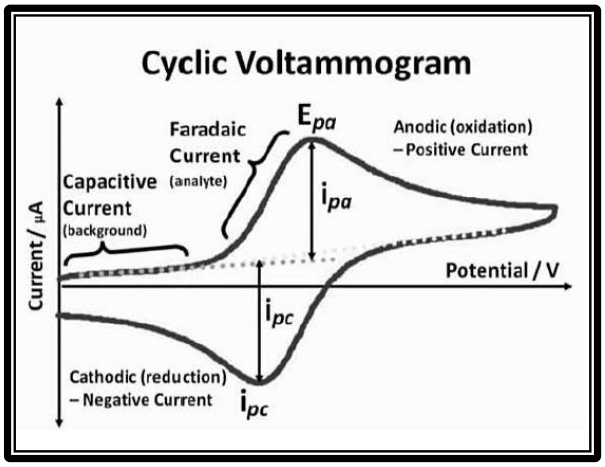

Figure 3.21 A typical I-V plot of cyclic voltammetry experiment [50].

In the present study, Cyclic Voltammetry (CV) was performed using a Solartron 1287 electrochemical interface and 1260 impedance gain phase analyzer (Figure 3.22). The measurement was taken by sandwiching polymeric gel electrolyte films between two stainless steel electrodes sweeping over a frequency range of 32 MHz to 0.1 Hz with 10 mV input of AC amplitude with 50mV scan rate.

Figure 3.22 Solartron 1287 electrochemical interface with 1260 impedance gain phase analyzer.

3.3.8 Tensile Strength Characterization

This characterization is useful to measure the mechanical strength of the polymers and other materials. The tensile strength or mechanical strength is measured by plotting the stress-

strain curve. Various characteristics such as elastic limit (proportional limit), yield point elongation at break, fracture point, modulus of elasticity (Young's modulus) can be measured from the stress-strain curve. A typical stress-strain curve is shown in Figure 3.23.

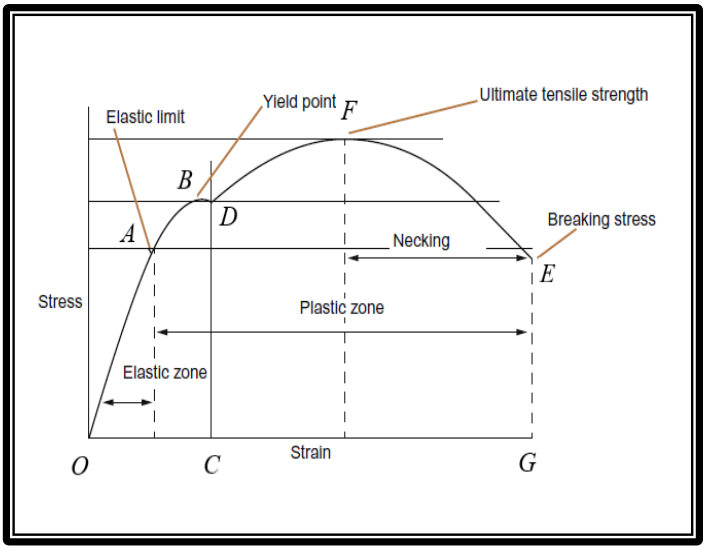

Figure 3.23 A typical stress-strain curve [51].

A detailed explanation of the stress-strain curve is given below.

Proportional limit: The linear part OA of the stress-strain curve indicates that the strain produced is directly proportional to applied stress. So, Hooke's law is obeyed up to point A. On removing stress, the original shape is removed (zero strain) represented by point O. The material is perfectly elastic up to stress corresponding to point A, which measures the elastic limit of the material.

Permanent Set: Beyond the elastic limit, strain increases more rapidly with stress as shown by a curve AB. In this region, the elongation of wire consists of both elastic and plastic deformation. So, on the removal of load, the material does not recover the original length. Some residual strain OC is crept in known as a permanent set.

Yield Point: Portion BD represents the strain of large values without any increase in stress. Point B at which a large increase in strain starts is called the Yield point.

Breaking stress: The extension beyond point D is observed due to plastic deformation which is produced due to shear stress that can only be produced by increasing the load gradually so that the DF portion is obtained. In this region, volume remains constant as the cross-sectional area decreases. Up to point F, the maximum deforming force or load applied

to the wire per its original cross-sectional area is called breaking stress also known as the ultimate strength of the material.

Breaking point: Beyond point F, the material is elongated even if the load is reduced. The material finally breaks at point E is called the breaking point.

In the present study, the mechanical strength of the gel polymer electrolyte films was tested by using mechanical tester model 5848, Singapore (Figure 3.24) at a strain rate of 100 mm/min with a maximum load of 10 N. During the tensile testing experiment, the sample having known length and cross-sectional area is clamped between two holders and the load is applied. Using an extensometer or strain gage, the elongation in the material can be measured

Figure 3.24 Mechanical tester (Model 5848, Singapore).

3.3.9 Electrical Properties

The electrical resistance is defined as the ratio of the applied voltage to current flow across the sample according to Ohm's law. This law is applicable only for the system that behaves as an ideal resistor which is a function of direct current (dc) and independent of frequency. For complex circuit elements, impedance measurement is more convenient to measure the resistance of the material [52]. Impedance spectroscopy measures the impedance of material with the application of a small ac signal. The resulting response will be frequency-dependent real and imaginary impedance values with their angles 'δ' between them [53].

In the Impedance spectroscopy, a small alternating sinusoidal signal with the voltage of a few millivolts V(t) is applied across a sample (Figure 3.25 (a)) and current i(t) is measured. The frequency of the current response i(t) is the same as that of applied voltage but it develops a phase difference between voltage and current. The voltage to current ratio, i.e. V(t)/i(t) is called the complex impedance of the sample denoted as Z(ω). The impedance is a function of frequency as V(t) and i(t) change with the frequency of the applied field. Measuring Z(ω) over a wide range of frequency and plotting of Z″(ω) against Z′(ω) called complex impedance plot or Nyquist plot [52]. Such a plot provides valuable information regarding electrical/electrochemical parameters such as dc conductivity, ac conductivity, dielectric permittivity, and electric modulus about the system.

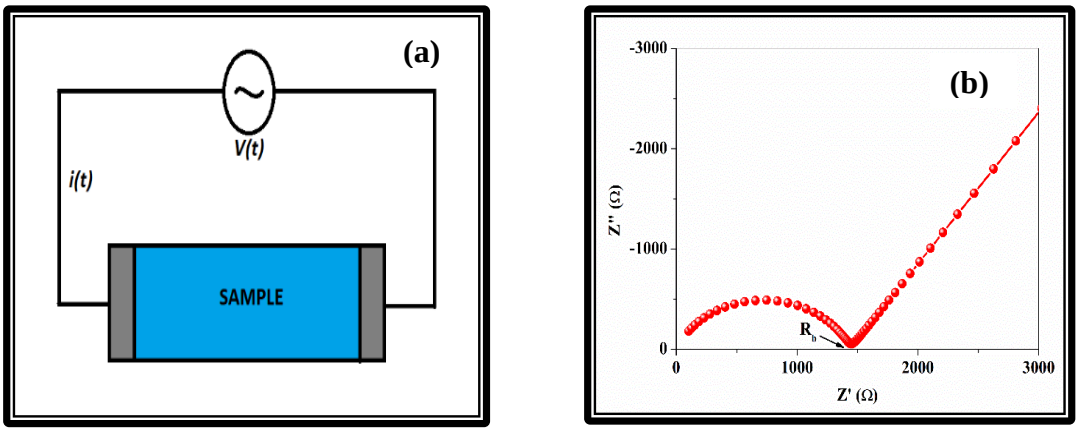

Figure 3.25 (a) A sample with an AC signal applied across it (b) A typical complex impedance plot.

A typical complex impedance plot is shown in Figure 3.25 (b). The intercept of the impedance plot with the X-axis ($Z'(\omega)$ data) corresponds to the resistance of the sample. The Y-axis ($Z''(\omega)$ data) corresponds to reactance. The electrical conductivity can be calculated from the bulk resistance and known dimensional parameters of the system. The expression for the same is given below

$$\sigma = \frac{t}{A} \cdot \left(\frac{1}{R_b} \right) \tag{3.10}$$

where t is the thickness of the sample, A is the contact area of electrode-electrolyte, R_b is bulk resistance. Other parameters such as temperature-dependent conductivity, Complex ac conductivity ($\sigma^*(\omega)$), complex dielectric permittivity ($\varepsilon^*(\omega)$) and complex electric modulus ($M^*(\omega)$) [54] can be evaluated from complex impedance ($Z^*(\omega)$) which provides ion

conduction mechanism and different relaxation processes within the materials [55]. The relation between all parameters is already discussed in Chapter 2.

In the present study, the complex impedance measurement is carried out using a Solartron SI-1260 Impedance Gain/Phase Analyser (Figure 3.26 (a)) in the frequency range 1 Hz to 32 MHz at different temperatures 303 K – 348 K. The polymer samples were sandwiched between two stainless steel blocking electrodes used as a cell for the measurement. The image of the sample holder is shown in Figure 3.26 (b).

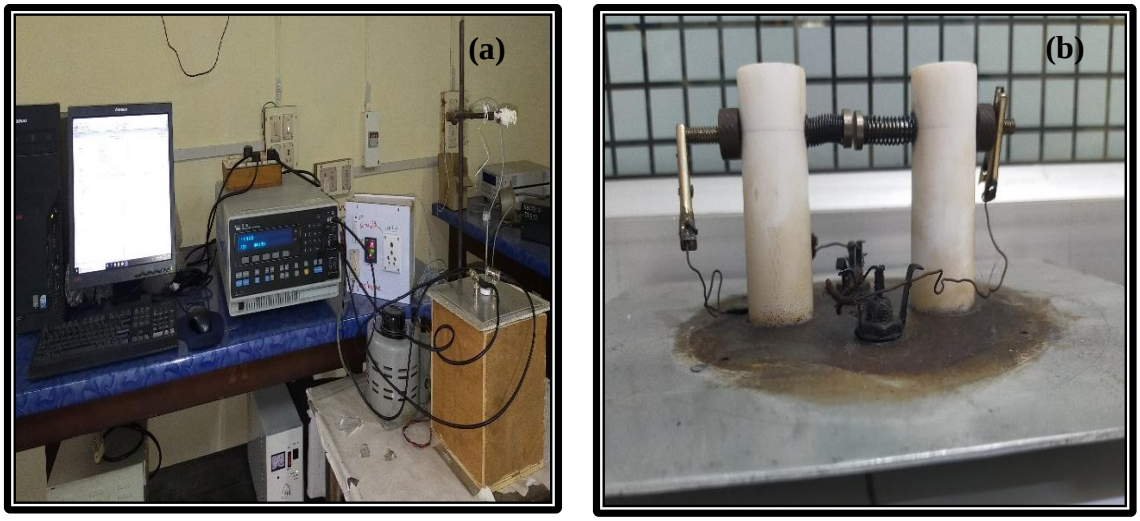

Figure 3.26 (a) Solartron SI-1260 Impedance Gain/Phase Analyser interfaced with computer (b) Sample holder.

References

[1] K. Karuppasamy, R. Antony, S. Alwin, S. Balakumar, and X. Sahaya Shajan, "A Review on PEO Based Solid Polymer Electrolytes (SPEs) Complexed with LiX (X=Tf, BOB) for Rechargeable Lithium Ion Batteries," *Mater. Sci. Forum*, vol. 807, pp. 41–63, 2015, doi: 10.4028/www.scientific.net/MSF.807.41.

[2] L. Long, S. Wang, M. Xiao, and Y. Meng, "Polymer electrolytes for lithium polymer batteries," *J. Mater. Chem. A*, vol. 4, no. 26, pp. 10038–10069, 2016, doi: 10.1039/C6TA02621D.

[3] R. Miao *et al.*, "PVDF-HFP-based porous polymer electrolyte membranes for lithium-ion batteries," *J. Power Sources*, vol. 184, pp. 420–426, Oct. 2008, doi: 10.1016/j.jpowsour.2008.03.045.

[4] A. Manuel Stephan and K. S. Nahm, "Review on composite polymer electrolytes for lithium batteries," *Polymer (Guildf).*, vol. 47, no. 16, pp. 5952–5964, 2006, doi: https://doi.org/10.1016/j.polymer.2006.05.069.

[5] A. Manuel Stephan, S. Gopu Kumar, N. G. Renganathan, and M. Anbu Kulandainathan, "Characterization of poly(vinylidene fluoride–hexafluoropropylene) (PVdF–HFP) electrolytes complexed with different lithium salts," *Eur. Polym. J.*, vol. 41, no. 1, pp. 15–21, 2005, doi: https://doi.org/10.1016/j.eurpolymj.2004.09.001.

[6] R. Subadevi, M. Sivakumar, S. Rajendran, H.-C. Wu, and N.-L. Wu, "Development and characterizations of PVdF-PEMA gel polymer electrolytes," *Ionics (Kiel).*, vol. 18, no. 3, pp. 283–289, 2012, doi: 10.1007/s11581-011-0629-0.

[7] L. N. Sim, S. R. Majid, and A. K. Arof, "Characteristics of PEMA/PVdF-HFP blend polymeric gel films incorporated with lithium triflate salt in electrochromic device," *Solid State Ionics*, vol. 209–210, pp. 15–23, 2012, doi: https://doi.org/10.1016/j.ssi.2011.11.035.

[8] K. B. M. Isa *et al.*, "Lithium ion conduction and ion–polymer interaction in PVdF-HFP based gel polymer electrolytes," *Solid State Ionics*, vol. 268, pp. 288–293, 2014, doi: https://doi.org/10.1016/j.ssi.2014.10.012.

[9] X. Flora, M. Ulaganathan, and S. Rajendran, "Role of Different Plasticizers in Li-Ion Conducting Poly(Acrylonitrile)-Poly(Methyl Methacrylate) Hybrid Polymer Electrolyte," *Int. J. Polym. Mater.*, vol. 62, pp. 737–742, Jun. 2013, doi: 10.1080/00914037.2013.769235.

[10] C. M. Mathew, K. Kesavan, and S. Rajendran, "Analysis of plasticizer influence in Poly(vinyl acetate)/Poly(vinylidene fluoride) polymer blend electrolyte," *Ionics (Kiel).*, vol. 20, no. 3, pp. 439–443, 2014, doi: 10.1007/s11581-014-1076-5.

[11] K. Sawai, Y. Iwakoshi, and T. Ohzuku, "Carbon materials for lithium-ion (shuttlecock) cells," *Solid State Ionics*, vol. 69, no. 3, pp. 273–283, 1994, doi: https://doi.org/10.1016/0167-2738(94)90416-2.

[12] A. Arya and A. Sharma, "Polymer electrolytes for lithium ion batteries: a critical study," *Ionics (Kiel).*, vol. 23, pp. 497–540, Jan. 2017, doi: 10.1007/s11581-016-1908-6.

[13] B. Kumar and L. G. Scanlon, "Polymer-ceramic composite electrolytes," *J. Power Sources*, vol. 52, no. 2, pp. 261–268, Dec. 1994, doi: 10.1016/0378-7753(94)02147-3.

[14] P. A. R. . Jayathilaka, M. A. K. . Dissanayake, I. Albinsson, and B.-E. Mellander, "Effect of nano-porous Al_2O_3 on thermal, dielectric and transport properties of the $(PEO)_9LiTFSI$ polymer electrolyte system," *Electrochim. Acta*, vol. 47, no. 20, pp. 3257–3268, 2002, doi: https://doi.org/10.1016/S0013-4686(02)00243-8.

[15] B. Luo, X. Wang, Y. Wang, and L. Li, "Fabrication, characterization, properties and theoretical analysis of ceramic/PVDF composite flexible films with high dielectric constant and low dielectric loss," *J. Mater. Chem. A*, vol. 2, no. 2, pp. 510–519, 2014, doi: 10.1039/C3TA14107A.

[16] R. C. Agrawal and G. P. Pandey, "Solid polymer electrolytes: materials designing and all-solid-state battery applications: an overview," *J. Phys. D. Appl. Phys.*, vol. 41, no. 22, p. 223001, 2008, doi: 10.1088/0022-3727/41/22/223001.

[17] B. D. Cullity, *Elements of x-ray diffraction*, 2nd Editio. Reading, MA : Addison-Wesley Publishing Company, Inc., 1978.

[18] L. Smart and E. A. Moore, *Physical Methods for Characterizing Solids*, *Solid State Chemistry: An Introduction*. New York: Taylor & Francis, 2005.

[19] W. H. Bragg and W. L. Bragg, *The crystalline state*. Cornell University Press, 1965.

[20] W. L. BRAGG, "The Specular Reflection of X-rays.," *Nature*, vol. 90, no. 2250, p. 410, 1912, doi: 10.1038/090410b0.

[21] B.D. Cullity, *Elements of X-Ray Diffraction, Reading*. Massachusetts: Addison-Wesley Publishing Company, Inc., 1956.

[22] C. NB, D. LH, and W. SE, *Introduction to infrared and Raman spectroscopy. Academic Press, New York*. New York: Academic Press, 1975.

[23] G. PR and de H. JA, *Fourier transform infrared spectroscopy*. New York: Wiley, 1986.

[24] S. M. Ashraf, S. Ahmad, and U. Riaz, *Experiments in Materials Science and Materials Chemistry-I: A Laboratory Manual of Polymers*. New Delhi: I.K. International Publishing House Pvt. Ltd., 2009.

[25] H. H. Willard, J. A. Dean, and J. A. Dean, *Instrumental Methods of Analysis*. Fourth ed.: Affiliated East Coast Press Pvt. Ltd., 1965.

[26] H. G, H. W, and F. H-J., *Differential Scanning Calimetry: An Introduction for Practitioners.* Berlin, Germany: Springer-Verlag, 1996.

[27] A. Karmakar and A. Ghosh, "Charge carrier dynamics and relaxation in (polyethylene oxide-lithium-salt)-based polymer electrolyte containing 1-butyl-1-methylpyrrolidinium bis(trifluoromethylsulfonyl)imide as ionic liquid," *Phys. Rev. E*, vol. 84, no. 5, p. 51802, Nov. 2011, doi: 10.1103/PhysRevE.84.051802.

[28] H. PJ, R. M, and W. FW, *Differential thermal analysis and differential scanning calorimetry*, Handbook o. The Netherlands: Elsevier Science BV, 1998.

[29] W.W. Wendlandt, *Thermal Methods of Analysis*, Second ed. York: Wiley-Interscience, 1974.

[30] L. H. Sperling, *Introduction to Physical Polymer Science*, Second ed. Singapore: John Wiley & Sons, Inc., 1993.

[31] R. L. Danley, "New heat flux DSC measurement technique," *Thermochim. Acta*, vol. 395, no. 1, pp. 201–208, 2002, doi: https://doi.org/10.1016/S0040-6031(02)00212-5.

[32] A. GUPTA, "EXPERIMENTAL STUDIES ON ION CONDUCTING POLYMER ELECTROLYTES," JAYPEE UNIVERSITY OF ENGINEERING AND TECHNOLOGY, 2013.

[33] A. R. West, *Elements of Solid State Chemistry*. New York: Wiley, 1987.

[34] C. R. Brundle, J. C. A. Evans, and S. Wilson, *Encyclopaedia of Materials Characterization*. USA: Butterworth Heinemann, a division of Reed Publishing (USA), Inc., 1992.

[35] W. Jin, W. Xu, H. Liang, Y. Li, S. Liu, and B. Li, "1 - Nanoemulsions for food: properties, production, characterization, and applications," in *Nanotechnology in the Agri-Food Industry*, A. M. B. T.-E. Grumezescu, Ed. Academic Press, 2016, pp. 1–36.

[36] J. Goldstein, *Scanning electron microscopy and X-ray Microanalysis*. 689 Seiten: Kluwer Acdacemic Plenu Publishers, 2003.

[37] A. R. Clarke, *Microscopy techniques for materials science*. Cambridge England.: CRC press, Woodhead Publisher Limited, 2002.

[38] S. K. Chaurasia and A. Chandra, "Organic-inorganic hybrid electrolytes by in-situ dispersion of silica nanospheres in polymer matrix," *Solid State Ionics*, vol. 307, pp. 35–43, 2017, doi: https://doi.org/10.1016/j.ssi.2017.05.003.

[39] R. Agrawal and R. K. Gupta, "Superionic Solids: Composite Electrolyte Phase - An Overview," *J. Mater. Sci.*, vol. 34, pp. 1131–1162, Mar. 1999, doi: 10.1023/A:1004598902146.

[40] R. Muchakayala, S. Song, S. Gao, X. Wang, and Y. Fan, "Structure and ion transport in an ethylene carbonate-modified biodegradable gel polymer electrolyte," *Polym. Test.*, vol. 58, pp. 116–125, 2017, doi: https://doi.org/10.1016/j.polymertesting.2016.12.014.

[41] C. Wagner, "Equations for transport in solid oxides and sulfides of transition metals," *Prog. Solid State Chem.*, vol. 10, pp. 3–16, 1975, doi: https://doi.org/10.1016/0079-6786(75)90002-3.

[42] M. Watanabe, M. Kanba, K. Nagaoka, and I. Shinohara, "Ionic conductivity of hybrid films based on polyacrylonitrile and their battery application," *J. Appl. Polym. Sci.*, vol. 27, no. 11, pp. 4191–4198, Nov. 1982, doi: 10.1002/app.1982.070271110.

[43] C. Tubandt, *Handbuch der experimentalphysik*. Leipzig : Akademische Verlagsgesellschaft, 1932.

[44] P. M. Blonsky, D. F. Shriver, P. Austin, and H. R. Allcock, "Complex formation and ionic conductivity of polyphosphazene solid electrolytes," *Solid State Ionics*, vol. 18–19, pp. 258–264, 1986, doi: https://doi.org/10.1016/0167-2738(86)90123-2.

[45] J. Evans, C. A. Vincent, and P. G. Bruce, "Electrochemical measurement of transference numbers in polymer electrolytes," *Polymer (Guildf).*, vol. 28, no. 13, pp. 2324–2328, 1987, doi: https://doi.org/10.1016/0032-3861(87)90394-6.

[46] J. B. Wagner, *Electrode processes in solid state ionics*. Dordrecht, Netherlands: Springer, 1976.

[47] J. Schoonman and A. J. H. Macke, "Electrical polarization of lead bromide crystals. I," *J. Solid State Chem.*, vol. 5, no. 1, pp. 105–110, 1972, doi: https://doi.org/10.1016/0022-4596(72)90016-3.

[48] T. Ishihara, T. Akbay, H. Furutani, and Y. Takita, "Improved oxide ion conductivity of Co doped $La_{0.8}Sr_{0.2}Ga_{0.8}Mg_{0.2}O_3$ perovskite type oxide," *Solid State Ionics*, vol. 113–115, pp. 585–591, 1998, doi: https://doi.org/10.1016/S0167-2738(98)00325-7.

[49] P. T. Kissinger and W. R. Heineman, "Cyclic voltammetry," *J. Chem. Educ.*, vol. 60, no. 9, p. 702, Sep. 1983, doi: 10.1021/ed060p702.

[50] "https://en.wikipedia.org/wiki/Linear_sweep_voltammetry." .

[51] J. P. Singh and S. Verma, "3 - Raw materials for terry fabrics," in *Woodhead Publishing Series in Textiles*, J. P. Singh and S. B. T.-W. T. F. Verma, Eds. Woodhead Publishing, 2017, pp. 19–28.

[52] T. Winie, A. K. Arof, and S. Thomas, *Polymer Electrolytes Characterization Techniques and Energy Applications*. Weinheim, Germany: Wiley-VCH Verlag GmbH & Co. KGaA, 2020.

[53] U. Retter and H. Lohse, "Electrochemical Impedance Spectroscopy," in *Electroanalytical Methods.*, F. Scholz., Springer, Berlin, Heidelberg, 2005.

[54] E. Barsoukov and J. R. Macdonald, *Impedance Spectrosopy: Theory ,Expeiment and Applications*, 2nd Editio. New Jersey, USA: John Wiley & Sons, Ltd, 2005.

[55] A. K. Jonscher, "Dielectric relaxation in solids," *J. Phys. D. Appl. Phys.*, vol. 32, no. 14, pp. R57–R70, 1999, doi: 10.1088/0022-3727/32/14/201.